Jet disturbances induced due to the interplay between wetting and turbulence

J. Ferrand,[1] L. Favreau,[1] S. Joubaud,[1,2] and E. Freyssingeas[1]
[1]*Univ Lyon, ENS de Lyon, CNRS, Laboratoire de Physique, F-69342 Lyon, France*
[2]*Institut Universitaire de France (IUF), 75005 Paris, France*

(Received 29 January 2021; accepted 19 November 2021; published 18 January 2022)

This article presents an experimental description of a jet disturbance occurring during tank draining. This disturbance is visible from the onset of the draining process, and in striking contrast with known jet instabilities, the jet resembles a chain of beads. These beads are generated at the orifice outlet before falling in free fall due to gravity. Such a disturbance is observed for flows through a circular hole, whose size is comparable to the capillary length. This phenomenon is observed when the initial fluid height in the tank exceeds a threshold value. This threshold height depends on the wettability of the outer surface of the tank bottom plate around the outlet orifice. Moreover, this disturbance is more pronounced and lasts longer when the surface around the orifice outlet is hydrophilic. Our experimental results suggest that this disturbance originates from the coupling between turbulence and wetting. Indeed, we believe that this new phenomenon is due to the combination of toroidal vortices generated in the outlet hole and the surface's wettability around the outlet orifice.

DOI: 10.1103/PhysRevFluids.7.014002

I. INTRODUCTION

Fluid's flow through an orifice as well as wetting of a fluid on a solid surface are two different aspects of fluid mechanics. The first study on tank draining through an orifice set at its bottom dates back nearly 400 years ago with Torricelli's work [1]. The flow rate equation of the draining fluid was set 100 years later by Bernoulli [2]. Since these seminal studies, many works have been carried out on this particular topic because of its importance in many natural and industrial processes [3–10]. On the other hand, the first investigation of the wetting of a solid surface by a liquid goes back a little more than 200 years ago, with the article of Young [11]. This work was the first attempt to propose a quantitative description of this phenomenon. Here again, because surface wetting plays an important role in many natural and industrial phenomena, for the last 200 years wetting has been studied extensively [12–14]. Nevertheless, despite 200 years of coexistence and many studies showing evidence that wetting properties could affect macroscopic flows [15–19], no investigations had considered the effect of wetting on tank draining. It has been only very recently [20] that a study has shown that for holes whose diameter is of the order of the capillary length, fluid wetting conditions on the outer surface around the outlet orifice strongly modify the exit flow rate and thus the emptying time.

Here we report a new striking effect of wetting on draining through an orifice that is the existence of a jet shape disturbance, starting at the onset of the flow. This disturbance consists in a modulation of the jet shape of short length along its axis. It occurs from the flow onset, right at the hole outlet, as shown in Fig. 1 and Fig. 2. To our knowledge such a phenomenon has never been described so far. In the following, we will show that this disturbance is due to the combination of both turbulence and wetting.

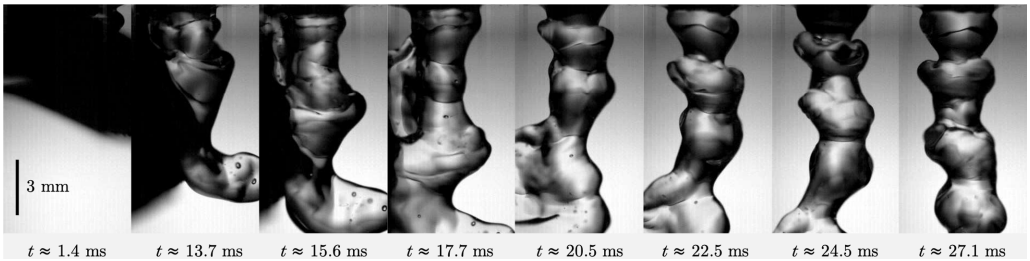

FIG. 1. Snapshots of the jet during the first milliseconds of the tank draining process through an orifice [$r_0 = 1.75$ mm, $h_0 = 10$ cm, hydrophilic glass surface; $t = 0$ s corresponds to the hole opening; $\mathrm{Re}(t = 0) \sim 4300$]. Images extracted from a movie recorded at 80 000 fps. (The movie from which these pictures were extracted can be seen in Section 2 of the Supplemental Material [35].) The top of the images corresponds to the top of the jet, i.e., the flow is from top to bottom of the figure; the images are cut right at the level of the hole outlet.

II. EXPERIMENTAL SETUP

The experimental device consists of a square tank of side 10 cm, whose bottom is a 2-mm-thick plate, in which a calibrated circular hole of radius r_0 is drilled at its center, here $r_0 = 1.75$ mm (see Section 1 of the Supplemental Material [35]). Experiments are carried out using distilled water at 25 °C (density $\rho = 997\ \mathrm{kg\,m^{-3}}$, dynamical viscosity $\eta = 0.89$ mPa s, and air-water surface tension $\gamma = 72\ \mathrm{mN\,m^{-1}}$). The tank is filled up to an initial height h_0 (that ranges between 11 and 2 cm); the fluid is let at rest a few minutes before opening the hole at $t = 0$ s. An electronic scale accurate to 0.1 g (KERN 532) placed 20 cm below the tank measures the drained mass of fluid as a function of time at a sample rate of 5 Hz. The drained mass $m(t)$ is converted into drained volume $V(t)$, $V(t) = m(t)/\rho$, where ρ is the fluid density and the flow rate $Q(t)$ is computed [$Q(t) = dV/dt$]. In this article, we also use the output fluid velocity, $v_{\mathrm{drain}}(t) = Q(t)/(\pi r_0^2)$. The global features of the disturbances are observed by means of a charge-coupled device (CCD) camera (Basler acA2000-165um) and a macro lens (18–108 mm) and recorded between 10 and 200 frames per second (fps). The jet shape at the beginning of the draining, the dynamics of the meniscus as well as the evolution of the jet are imaged from 6000 to 80 000 fps thanks to a high-speed camera (Phantom v 2511) and an objective (Nikon ED -AF Micro NIKKOR 200mm 1:4 D).

With the used experimental parameters, assuming the exit velocity of the fluid at the hole opening, i.e., at $t = 0$ s v_T, is given by Torricelli's model $v_T = \sqrt{2gh_0}$, the Reynolds number at the onset of the flows $\mathrm{Re} \approx 2r_0\rho v_T/\eta$ is estimated between ∼2200 and ∼5000. The Weber number, $\mathrm{We} \approx (2r_0\rho v_T^2)/\gamma$, should range between ∼35 and ∼100. Due to dissipation, the real value of the outflow velocity is smaller than v_T and therefore the expected values of Re and We should be slightly smaller than those given here but of the same order of magnitude. According to the Weber number of these flows, it is expected to be in the jetting regime [8,21].

Results reported in this article are obtained for flows through five bottom plates whose wettability of the outer surface is different. The wettability of a solid surface for water is defined as the quantity $\gamma \cos\theta_s$, where θ_s is the characteristic static contact angle between the solid surface and distilled water [22]. Hence water wets all the more the solid surface since its wettability is high, i.e., θ_s is low. The different materials used in this study are as follows: hydrophilic glass ($\theta_s \sim 13°$), Plexiglas [i.e., poly(methyl methacrylate), $\theta_s \sim 64°$], two kinds of PVC; PVC-1 ($\theta_s \sim 68°$), PVC-2 ($\theta_s \sim 70°$), and hydrophobic glass (coated glass with Rain-X original glass water repellent, $\theta_s \sim 88°$). Except for experiments presented in Sec. IV, which were carried out with PVC-2 plates, all other experiments performed with PVC plates were conducted with PVC-1. Moreover, it should be noticed that when the outer surface of the tank bottom plate is of hydrophobic glass, the inner surface of this bottom plate is of hydrophilic glass.

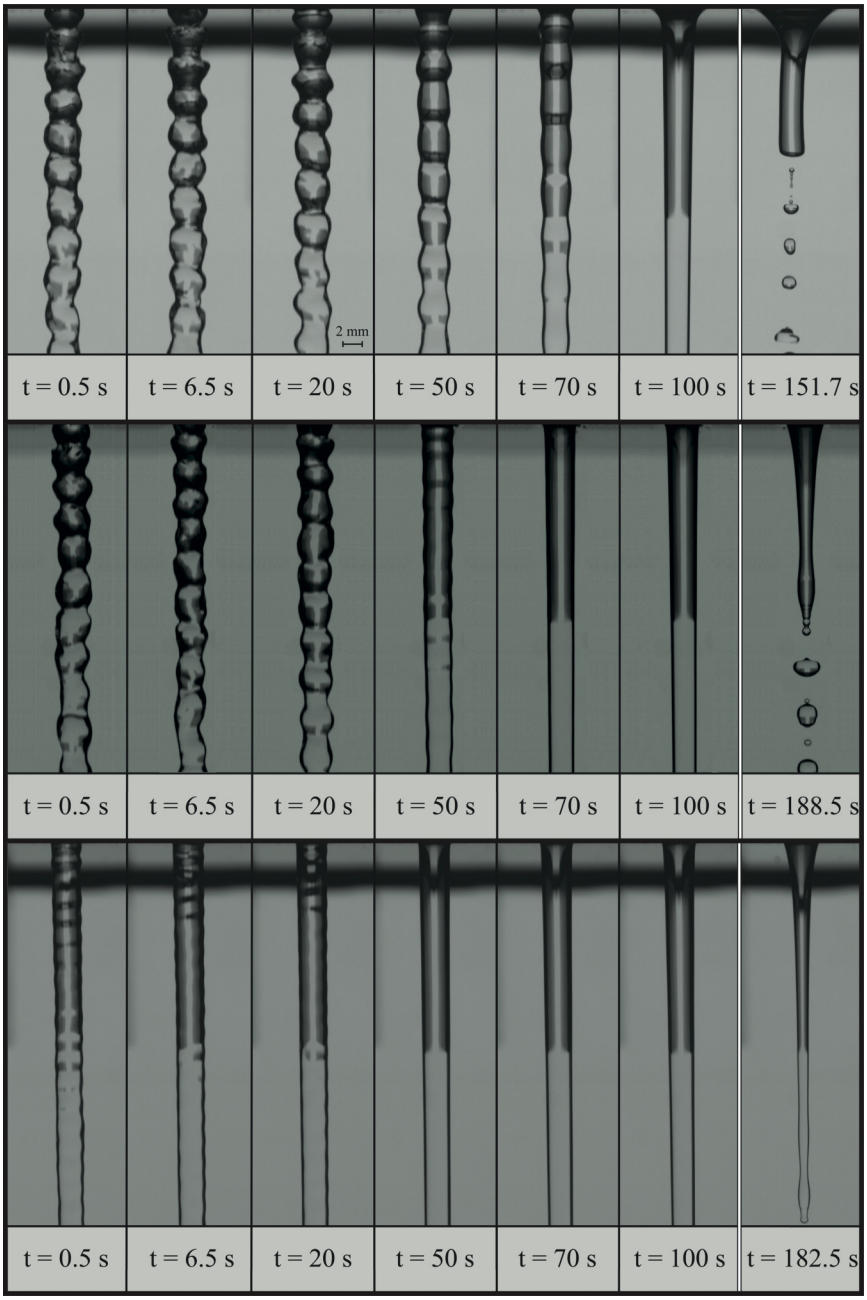

FIG. 2. Snapshots of the jet at different times during tank draining through an orifice for three wetting conditions ($r_0 = 1.75$ mm, $h_0 = 10$ cm; $t = 0$ is the hole opening). The top of the images corresponds to the top of the jet, i.e., the flow is from top to bottom of the figure; the images are cut right at the level of the hole outlet. These images show ∼40 mm of the top of the jet from the hole outlet. Top: hydrophilic glass surface ($\theta_s \sim 13^\circ$), Re($t = 0$) ∼ 4300; middle: Plexiglas surface ($\theta_s \sim 64^\circ$), Re($t = 0$) ∼ 3900; bottom: hydrophobic glass surface ($\theta_s \sim 88^\circ$), Re($t = 0$) ∼ 4000. It should be noticed that the last picture of each row corresponds to the end of the draining process, indicating that the total flow duration varies with θ_s [20]. (Movies from which these pictures are extracted were recorded at 50 fps and are available in the Supplemental Material [35]; see description in section 2.) Characteristics of these disturbances are displayed in Table I.

III. A NEW JET DISTURBANCE

This section describes experiments carried out with the same initial fluid height in the tank ($h_0 = 10$ cm) for different wettability properties of the outer surface of the tank bottom plate. For each wettability condition, the tank draining was repeated several times and each time the outgoing jet was recorded at 50, 200, or 80 000 fps. When recorded at 50 or 200 fps, the jets are shot throughout the draining process, when recorded at 80 000 fps, they are shot only for the first two seconds of the draining process. Here it should be noticed that, in agreement with our previous study [20], the jet behavior only depends on the wettability of the outer surface of the bottom plate; the wettability of the inner surface of the bottom plate plays no significant role in the jet behavior at the hole exit or the wettability inside the hole.

Figure 1 displays snapshots of the jet at the tank outlet taken within the first tens of milliseconds of the draining process in the case of the hydrophilic glass surface (movies as well as pictures showing the jets at the onset of the drainage process for all wettability conditions are shown in sections 2 and 3 of the Supplemental Material [35]). Pictures of Fig. 1 are extracted from a movie recorded at 80 000 fps. The first image in this figure displays the jet ∼1.4 ms after the hole opening [$\mathrm{Re}(t = 0) \sim 4300$]. In this image, the liquid starts to pop out of the tank although the cap closing the hole is not fully detached from the bottom surface yet. The last image of this set is about 27 ms after the hole opening. On this image, the jet exhibits a bead chain like shape. At this time, the jet length from the hole exit is about 2.2 cm; the bottom end of the jet has thus not reached the ground yet. For all wettability conditions that were used in this work, the disturbance setup is always very fast after the hole opening. In all cases, it can be noticed that bulges and beads are formed as soon as the liquid starts to pop out of the tank and the disturbance is fully established in a time of the order of 25–30 ms (then the jet exhibits a bead chain like shape). At that precise moment, the jet length is still only ∼3 cm and has not hit the ground yet.

Figure 2 shows snapshots from $t \approx 0.5$ s after the hole opening until the appearance of the dripping regime. All these pictures are extracted from movies recorded at 50 or 200 fps, and show ∼40 mm of the jet from the hole outlet. For all wettability, it is observed a disturbed jet, which disappears after a while in favor of a stable jet, well before the dripping regime. Therefore, one observes that from the very early stages of the flow, typically about 25–30 ms after the flow onset and then for several tens of seconds, the jet free surface is modulated from the hole outlet by variations of the jet radius along its vertical axis z. This modulation consists of a regular pinching of the jet along z, making bulges all along the jet from the hole outlet. During this period, hence over four orders of magnitude in time, the jet appears to be a continuous string of beads.

This disturbance alters the jet shape according to the distance from the tank outlet z and time t (where $z = 0$ is taken at the hole outlet level and $t = 0$ s at the hole opening). Qualitative observation of these figures enables some of the features of this disturbance to be determined. The time duration of the transient process does not seem to depend on the wettability (at least, the obtained results do not allow us to observe any significant effect). The distance between two consecutive pinching points of the jet seems to be weakly dependent on the wettability; it appears to be slightly larger for the more hydrophilic conditions. Moreover, one also notices that the distance between two consecutive pinching points increases as one gets further away from the outlet hole. At first sight this parameter seems to be almost constant during the main part of the disturbance, it starts to increase strongly as the disturbance approaches its end. Throughout the disturbance duration, the amplitude of the jet modulation, which here is defined as the difference between the diameter of the beads and the diameter of the pinches, is all the larger since the surface is more hydrophilic. This amplitude decreases with time, until it reaches 0. The time, t_{stop}, at which the modulation vanishes indicates the disappearance of the bead string shape and thus sets the end of the disturbance. Hence t_{stop} is also the disturbance duration. This quantity increases with the surface wettability. Most striking, for the same experimental conditions, the ratio between t_{stop} and the draining duration t_{drain}, t_{stop}–t_{drain}, increases with surface wettability. The flow velocity at which the disturbance vanishes, $v_{\mathrm{drain}}(t_{\mathrm{stop}}) = v_{\mathrm{stop}}$, as well as the fluid height remaining in the tank at the transition toward a

TABLE I. Main features of the disturbance for four wetting conditions with the same initial height of fluid in the tank: $h_0 = 10$ cm. Column 1: measured values of the disturbance duration, t_{stop} (determined by image analysis of the movies; see details in section 5 of the Supplemental Material [35]). Column 2: measured values of the draining duration, t_{drain} (determined from elapsed mass data as a function of time). Column 3: ratio of disturbance duration with respect to the whole draining duration; t_{stop}-t_{drain}. Column 4: measured values of the fluid height remaining in the tank when the disturbance vanishes, $h(t_{stop}) = h_{stop}$ (determined from elapsed mass data as a function of time). Column 5: hydrostatic pressure at the end of the disturbance; $\rho g h_{stop}$. Column 6: measured values of the flow velocity at the end of the disturbance, $v_{drain}(t_{stop}) = v_{drain}(h_{stop}) = v_{stop}$ [determined from flow rate data, $Q(t_{stop})/(\pi r_0^2)$]. Column 7: Reynolds number at the end of the disturbance.

Material	t_{stop} (s)	t_{drain} (s)	t_{stop}/t_{drain}	h_{stop} (cm)	$P_{H\,stop}$ (Pa)	v_{stop} (m s^{-1})	Re_{stop}
Hydrophilic glass ($\theta_s \sim 13°$)	82 ± 0.5	151.7 ± 0.5	~54%	3.1 ± 0.1	~303	0.63 ± 0.01	~2200
Plexiglas ($\theta_s \sim 64°$)	65 ± 0.5	188.5 ± 0.5	~34%	4.5 ± 0.1	~440	0.68 ± 0.01	~2380
PVC-1 ($\theta_s \sim 68°$)	53 ± 0.5	188.0 ± 0.5	~28%	5.5 ± 0.1	~540	0.72 ± 0.01	~2500
Hydrophobic glass ($\theta_s \sim 88°$)	22 ± 0.5	182.5 ± 0.5	~12%	7.8 ± 0.1	~760	0.93 ± 0.01	~3250

stable jet, $h(t_{stop}) = h_{stop}$, are all the smaller since the surface wettability is high (more hydrophilic surfaces). Thereby, this disturbance develops all the more since the surface wettability is high. All these latter observations are indicated in Table I for four wetting conditions.

Looking at Fig. 2, one could think that this disturbance is a wave that develops along the jet. If this is the case, then it can already be stated that this disturbance is not the Rayleigh-Plateau instability. Indeed, whatever the wettability of outer surface, the distance between two jet pinches is of the order of 3–4 mm, thereby about 4 times smaller than the expected wavelength for Rayleigh-Plateau instability with such a jet radius [23,24]; $\lambda_{RP} \sim 2\pi\ r_0/0.697 \approx 15$ mm. Because of the shape of the disturbance, one could believe this is a "Bamboo wave," related to the shear in the air [25–27]. However, since the disturbance described here is already fully developed a few milliseconds after the onset of the flow, with a jet length from the hole outlet of the order of 2 cm, this is very unlikely. Moreover, in this experiment, the water jet is not confined in a pipe, it falls into an air volume of several cubic meters (the closest wall is 50 cm away). Consequently, it is difficult to figure out how the mechanism triggering the Bamboo instability (hydrodynamic-lubrication forces) could be set in motion so quickly in this case. Another possible interpretation would be that this wave is due to the impact of the jet on the ground (the container bottom into which the flowed liquid falls). This does not hold. The distance between the hole outlet and the container was changed between 10 and 40 cm (i.e., the total jet length), and this had no effect on the disturbance features. Furthermore, this disturbance is set in a very short time after the hole opening whereas the jet has not reached the "ground" yet. Consequently, for all these reasons, we do not believe that this disturbance is a wave that develops along the jet.

Figure 3 displays snapshots of the jet extracted from a movie recorded at 80 000 fps for a hydrophilic glass surface, a few seconds after the flow onset. This figure shows the evolution of the jet disturbance over a duration of about 2.4 ms. This set of pictures clearly shows the appearance of a new bead at the top of the jet. The two horizontal yellow lines in each image of the figure indicate the position of two pinches along the jet. In the first image ($\tau = 0$ s), the first pinch is just below the hole outlet and the second one about 2 cm lower. On this set of images, it is clearly seen that these two pinches are falling down with time, while a new bead is appearing right at the tank outlet. The last image of this series coincides with the complete exit of this bead from the orifice, with the appearance of a new pinch at the hole outlet ($\tau \approx 2.4$ ms). The beads are popping out of the tank with the liquid flowing out. This leads us to the idea that the beads are generated at the tank outlet and then drop in free fall; there is a continuous production of beads coming out of the hole. Moreover, it can also be noticed that the lowest pinch drops faster than that closest to the hole. The

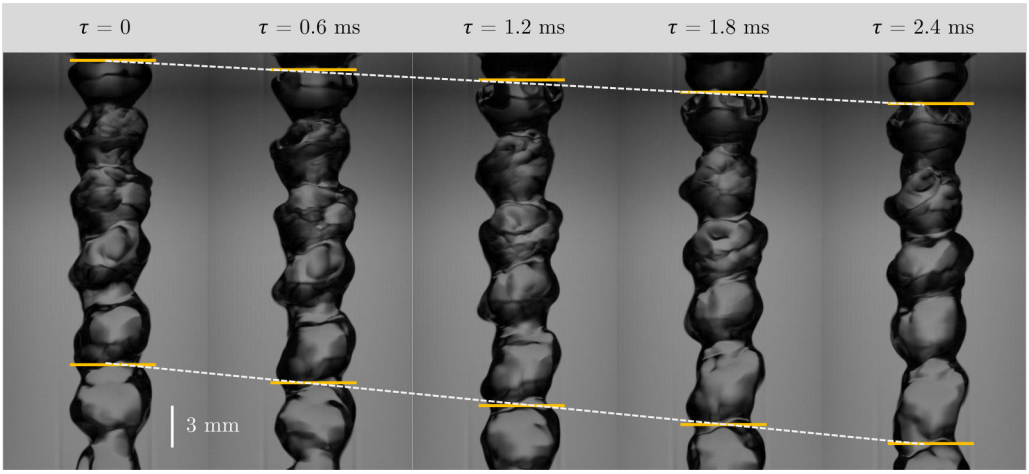

FIG. 3. Snapshots of the jet extracted from a movie recorded at 80 000 fps in the case of a hydrophilic glass surface ($r_0 = 1.75$ mm, $h_0 = 10$ cm; this movie can be seen in the Supplemental Material [35]). The top of the images corresponds to the top of the jet, i.e., the flow is from top to bottom of the figure; the images are cut right at the level of the hole outlet. Here $\tau = 0$ s is set at the beginning of a bead appearance at the tank outlet, thus for the first picture of this figure. The last picture of this set corresponds to the end of the bead appearance since a new pinch can be seen right underneath the hole outlet. The temporal spacing between two successive snapshots is 0.6 ms. The two dashed white lines are just guides for the eyes to show the fall of the pinches with time.

closest pinch to the outlet hole falls at a velocity of about 1.32 m s^{-1} (which roughly corresponds to the fluid velocity at the hole exit) while the furthest pinch falls at a velocity of about 1.9 m s^{-1}. This difference in velocity simply reflects the effect of gravity, which accelerates the jet. This explains why the beads are more elongated when away from the hole.

The process by which the beads appear is confirmed with Fig. 4. This figure shows snapshots of a zone of 3 mm high and 6 mm width at the hole outlet over a duration of 2.4 ms. These snapshots are extracted from movies recorded at 80 000 fps, both for hydrophilic glass and Plexiglas surfaces, respectively. For Figs. 4(a) and 4(b), the first picture of each set is chosen as the time origin; $\tau = 0$ s (i.e., the picture in the top left corner). This picture shows the beginning of a bead appearance at the top of the jet. On these pictures, it is initially seen the fluid emerging from the orifice and expanding laterally due to wetting; a growth of the jet radius in $z \approx 0$ is then observed. This growth phase seems to be fast at first before slowing down. Then the jet radius retracts quickly to form a pinch. At time τ_0 the jet shape has returned to that it had at $\tau = 0$ s. The retraction phase is shorter than the growth phase. Both τ_0 the duration of the bead appearance, as well as τ_g and τ_r, the duration of the growth and retraction phases respectively, depend on surface wettability. τ_0 is shorter for Plexiglas than for hydrophilic glass, probably because the amplitude of the jet disturbance is larger for hydrophilic glass than for Plexiglas. Note that it can be seen that during the whole bead appearance process, the position of the triple contact line barely moves.

IV. PHASE DIAGRAM AND ORIGIN OF THE DISTURBANCE

To the best of our knowledge, such a jet disturbance has never been described before. Consequently, further investigations are performed to explore the conditions of the disturbance existence and figure out its origin.

Experiments where h_0 is varied from 11 to 2 cm demonstrate that the disturbance occurs or not at the flow onset depending on the initial height of fluid in the tank h_0. If the disturbance is

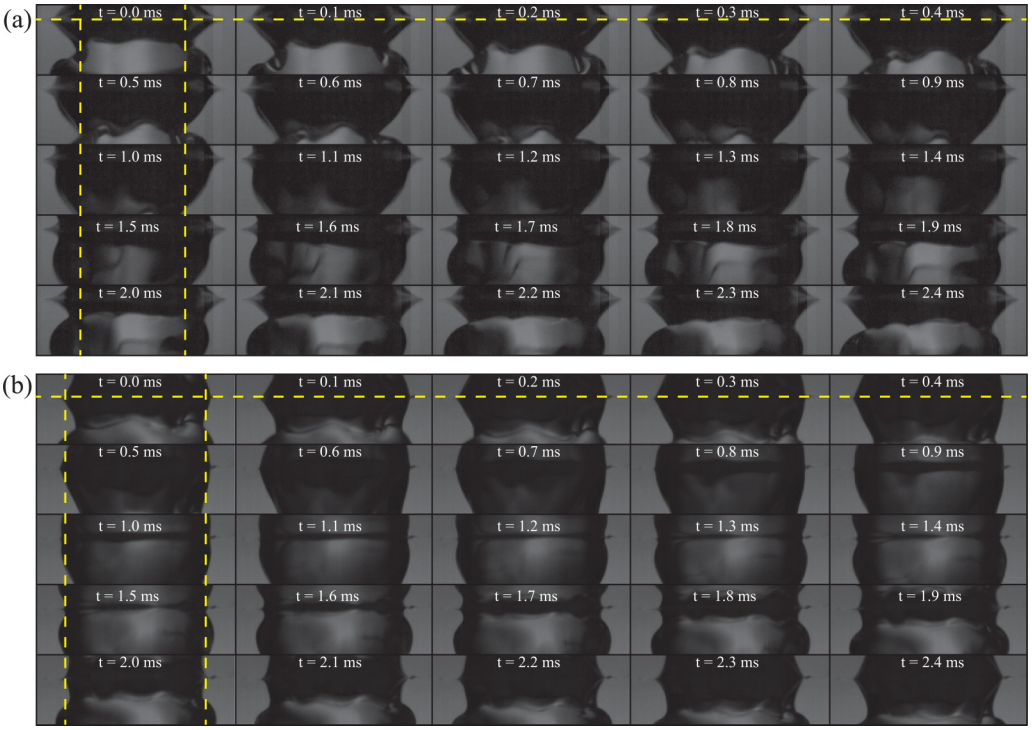

FIG. 4. Snapshots of a zone of 3 mm high and 6 mm width of the jet at the hole outlet at different times τ over a period of 2.4 ms; $\tau = t - t_0$, where t_0 is arbitrarily chosen at the beginning of the bead appearance, i.e., the time at which the bead starts to pop out. The top of the images corresponds to the top of the jet, i.e., the flow is from top to bottom of the figure; the images are cut right at the level of the hole outlet. Here the temporal spacing between two successive snapshots is 0.1 ms, corresponding to eight recorded pictures. The horizontal yellow dashed line corresponds to the outer surface of the tank bottom plate (the hole outlet level). The vertical yellow dashed lines locate the tank orifice (the hole diameter; $2r_0 = 3.5$ mm). (a) Case of the hydrophilic glass surface ($h_0 = 10$ cm, $r_0 = 1.75$ mm). $\tau = 0$ s corresponds to the image in the top left corner. Here $\tau_0 \sim 2.4$ ms; the growth phase takes about 75% of τ_0 (i.e., $\tau_g \sim 1.8$ ms) while the retractation phase is only 25% of the bead appearance duration τ_0 ($\tau_r \sim 0.6$ ms). (b) Case of the Plexiglas surface ($h_0 = 10$ cm, $r_0 = 1.75$ mm). $\tau = 0$ s corresponds to the picture in the top left corner. Here $\tau_0 \sim 2.2$ ms, the growth phase accounts for about 65% of τ_0 (i.e., $\tau_g \sim 1.4$ ms), while $\tau_r \sim 0.8$ ms.

not seen at the start of the flow, then it will never appear later on during the draining process. Therefore, this disturbance only occurs if h_0 exceeds h^*, a threshold height, that depends on the surface wettability. This is what is observed on the phase diagram displayed in Fig. 5. Of course, h^* corresponds to a threshold velocity v^*; $v^* \propto \sqrt{h^*}$, the disturbance exists as $v_{\text{drain}} > v^*$, and a threshold hydrostatic pressure P_H^*; $P_H^* \propto h^*$, the disturbance exists whether $P_H > P_H^*$ (Table IV). It can also be defined a critical Reynolds number, $\text{Re}^* = 2r_0\rho v^*/\eta$, depending on the outer surface wettability; Re^* varies between ~2250 and ~3150 (Table IV). It is therefore expected that in the disturbed regime the outgoing flow is turbulent, which is observed in the movies recorded thanks to the high-speed camera. For each wetting condition, the orange circles indicate the initial heights for which the flows are disturbed at the draining onset for more than 1 s, while the gray circles indicate h_0 conditions for which the flows are disturbed for less than 1 s at the flow onset or immediately stable. One notices that h^* is all the smaller since the wettability of the outer surface is high. This phase diagram clearly indicates that the surface wettability as well as the fluid outlet velocity are two of the parameters monitoring this disturbance. Here it is worthwhile to emphasize that some of

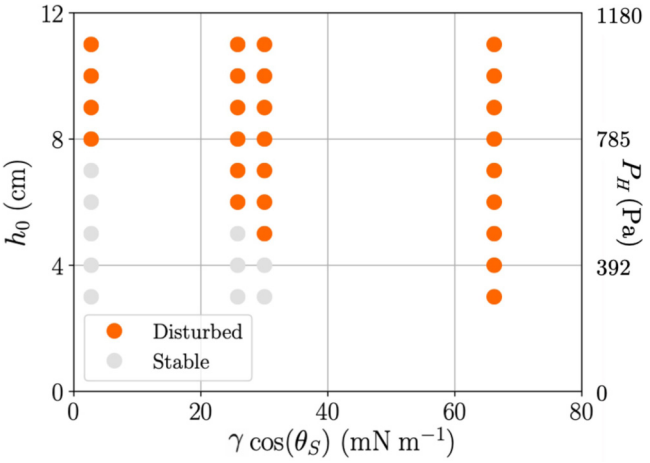

FIG. 5. Phase diagrams of the jet's shape, disturbed-stable, at the onset of water flows as a function of $\gamma \cos\theta_s$ (representing the outer surface wettability) and h_0 and P_H (circular sharp-edged hole, $r_0 = 1.75$ mm). Orange circles indicate the situations where the outlet jet exhibits the disturbance for at least the first second of the draining process.

the disturbance features are shared by all disturbed flows: bead string shape, existence depending on the fluid outlet velocity or the hydrostatic pressure, turbulent fluid motions inside the beads (this is visible in Figs. 1 and 3 and clearly obvious on the "high-speed" movies, e.g., on movies shown in Supplemental Material [35]), and transitory regime required for the disturbance to fully develop after the flow onset is always of the order of ∼25–30 ms (see section 3 of the Supplemental Material [35]). This latter characteristic suggests that the mechanism behind this disturbance is switched on as soon as the liquid flows out of the tank.

It is known that when a fluid flows through a pipe with a steeply varying cross section, the flow lines cannot change direction so suddenly. This causes the boundary layer to detach at the point where the section changes. As a result, this detachment of the boundary layer induces, downstream of the orifice, a contraction of the laminar jet with streamlines narrowing and a maximum speed of the fluid and all around this contracted jet a zone of turbulent fluid recirculation. This phenomenon of contraction of the jet cross-sectional area is known as *vena contracta* [28–31]. In this study, the tank section S is 10^{-2} m^2 and the hole section $S_0 = \pi r_0^2 \approx 10^{-5}$ m^2; hence there is a ratio of 1000 between these two sections, which corresponds well to an abrupt contraction. Moreover, the outlet orifice is a sharp-edged cylindrical hole, which amplifies the boundary layer detachment phenomenon. However, here the "small pipe" length is very short (2 mm) and afterwards the fluid flows in an open space; it is therefore likely that the turbulent zone is not confined. Nonetheless, an assumption that comes to mind is that turbulence driven by the boundary layer detachment at the orifice entrance leads to the formation of toroidal vortices that are advected by the flow toward the outlet of the hole and the outside. In this framework, it is imagined that this disturbance arises from the ejection of toroidal vortices through outlet hole, these vortex rings being generated by the boundary layer detachment at the hole inlet. Intuitively, each bead should correspond to one vortex ring. In a sense, the outlet hole would act as an "obstacle" on a laminar jet.

To probe this hypothesis, experiments are carried out using the same material for the tank bottom plate, with holes of different shapes. On the one hand, we use a plate 2 mm thick with a sharp-edged circular hole of 1.75 mm radius and, on the other hand, a plate 2 mm thick with a beveled-edge hole. In that later case, the hole entrance has a radius of 3 mm, while the hole outlet radius is still 1.75 mm, leading to a bevel making an angle with respect to horizontal $\theta_B \approx 58°$ ([see Fig. 3(a) in section 4 of the Supplemental Material [35]]. As set out in Sec. II, these bottom plates are made

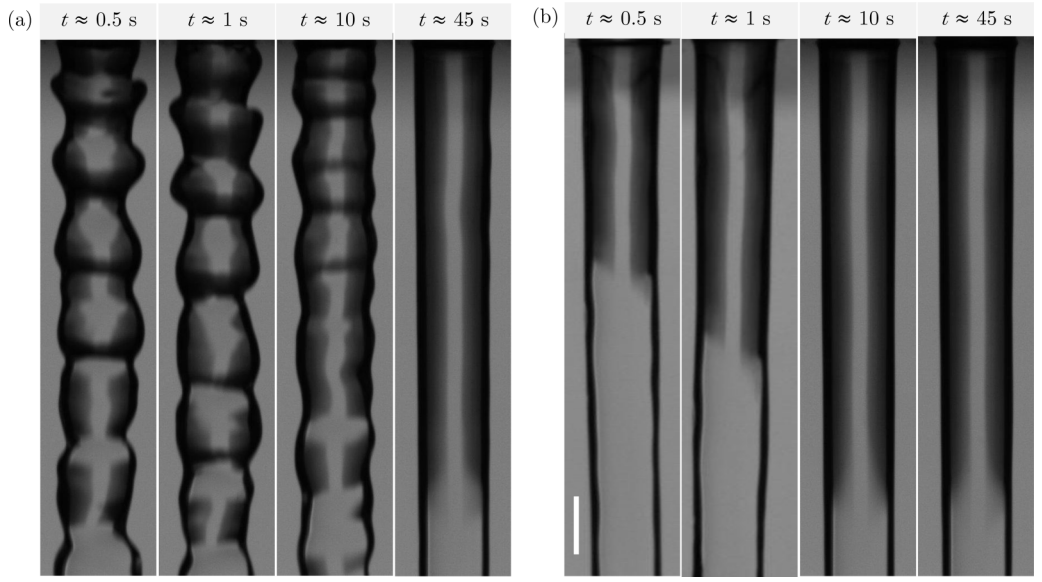

FIG. 6. For the two different orifices, snapshots of the jet at different times during draining process, from 0.5 to 45 s after the hole opening. The top of the images corresponds to the top of the jet, i.e., the flow is from top to bottom of the figure; the images are cut right at the level of the hole outlet. The two bottom plates, 2 mm thick, are made with the same PVC (PVC-2). Experiments are carried out under the same conditions; water at 25°C, and $h_0 = 9$ cm, $\mathrm{Re}(t = 0) \sim 3700$. (a) On the left side: flow through a sharp-edged cylindrical hole with radius $r_0 = 1.75$ mm. The existence of the disturbance of the jet is observed for the four pictures. (b) On the right side: flow through a beveled hole with an exit radius $r_0 = 1.75$ mm and an angle with respect to horizontal of 58°. There no trace of the disturbance is never seen; the jet is always stable. The white bar is 3 mm long and serves as a scale.

of PVC-2, the wettability of which is characterized by $\theta_s \sim 70°$. By using a beveled hole instead of a sharp-edged hole, it should prevent the streamlines from making a sharp turn as they enter into the hole, avoiding so the boundary layer detachment at the hole entrance and therefore creation of vortex rings. Consequently, this should inhibit the disturbance. For both orifices, experiments are carried out with initial fluid height h_0 ranging between 11 and 7 cm, and regardless of the value of h_0, the obtained results are identical. Disturbance is always seen for the sharp-edged hole, while it is never observed for the beveled hole. An example is shown in Fig. 6. This figure presents snapshots of the jet at different moments of the flow, from 0.5 to 45 s after the hole opening, for flows through the sharp edge hole and the beveled hole. Here experiments are performed with $h_0 = 9$ cm [$\mathrm{Re}(t = 0) \sim 3700$]. Pictures on the left side show the jet in the case of the sharp-edged cylindrical hole, it is observed a disturbed jet whose contour presents a bead chain like shape deformation [the first moments of this flow after the outlet orifice can be seen in Supplemental Material [35], Sec. 3; Fig. 2(d)]. The perturbation lasts ∼46.5 s while the whole draining duration is ∼175 s, and it stops when the height of fluid in the tank goes below ∼5.9 cm. The slight difference with the results presented above for PVC-1 plates is likely explained by the slight difference in wettability between the two used PVC. Pictures on the right side correspond to the case of the beveled hole. It is observed that the jet exhibits no deformation, in addition no disturbance is seen in the first milliseconds following the hole opening [see Fig. 3(b) in section 4 of the Supplemental Material [35]]; thus the jet is stable from the onset of the flow. Therefore, it can be asserted that a beveled hole inhibits the disturbance existence.

This confirms our hypothesis and provides us with a framework for understanding the origin of this disturbance. We believe that this disturbance originates from the combination of two distinct

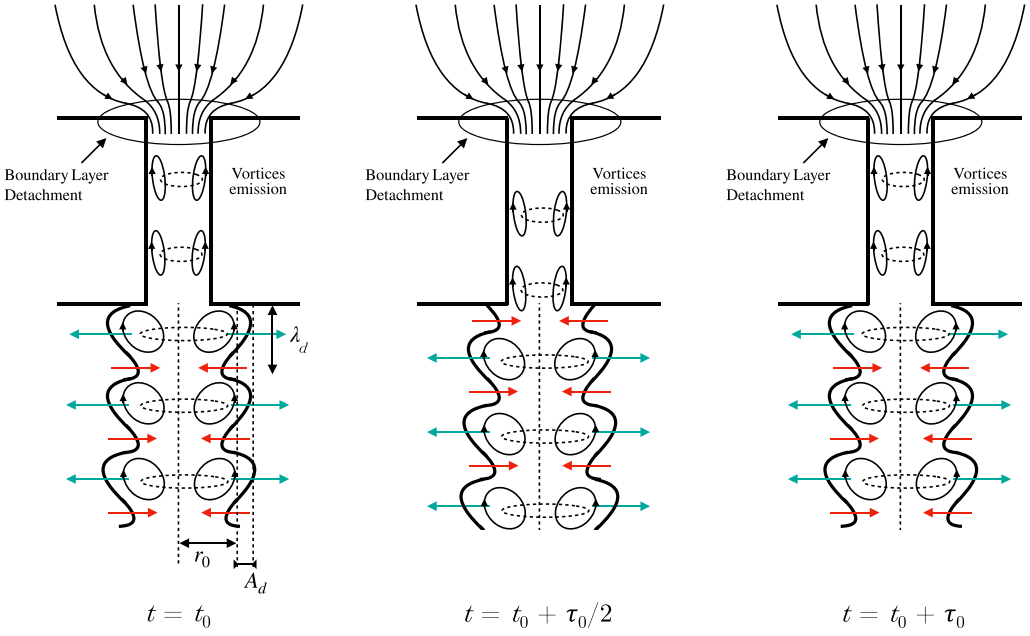

FIG. 7. Schematic representation of the disturbance. Toroidal vortices are created at the entrance of the tank outlet due to the detachment of the boundary layer. At $t = t_0$, a vortex has just popped out of the hole, the following vortex is still inside the hole, the outgoing flow at the orifice exit is laminar, and there the jet radius is minimum. At $t = t_0 + \tau_0/2$, a vortex is emerging from the hole, due to wetting and fluid horizontal velocity, the flowing liquid spreads out on the outer surface of the bottom plate and the radius of the jet at the hole exit grows. At $t = t_0 + \tau_0$, the vortex has exited the hole, the next one is still inside the hole, the outgoing flow at the orifice outlet is again laminar and downward, and the jet radius at the exit of the orifice has retracted and is minimum; the situation of $t = t_0$ is restored.

phenomena: turbulence generated by a periodic boundary layer detachment at the orifice entrance and wetting properties of the outer surface at the orifice outlet. This is illustrated schematically in Fig. 7. The first phenomenon induces the jet disturbance by creating toroidal vortices, which are then advected toward the hole exit. The second phenomenon plays a role on the lateral extension of the disturbance. On a hydrophilic material, water spreads out on the surface around the hole, over few millimeters, which allows wide lateral expansion of the vortices. Then, one expects a jet deformation of large amplitude and therefore beads of large volume. On a hydrophobic material, on the contrary, water flowing out from the tank does not wet much the surface around the hole and thereby vortices cannot extend laterally. This results in a jet deformation of small amplitude and therefore beads of small volume. However, from the phase diagram (Fig. 5) and the results shown in Tables I, III, and IV, it is obvious that the effect of wetting is much more subtle than just monitoring the disturbance amplitude. Note that in the framework of toroidal vortices formed at the orifice inlet, it can be imagined that the growth phase corresponds to the vortex lifetime, while the retraction phase corresponds to the waiting time between a vortex detachment and the beginning of the appearance of a new one. This view of the disturbance, however, might be a little too naive. One can imagine that vortices are also formed at the hole outlet and then the jet disturbance originates from the interaction of those two vortices, as seen in Ref. [32]. In both cases, however, the disturbance is due to turbulence induced by the hole.

V. CHARACTERISTICS OF THE JET DISTURBANCE AND TRANSITION DISTURBED-STABLE REGIME: EFFECT OF SURFACE WETTABILITY

As mentioned above, Fig. 1, the phase diagram (Fig. 5) and Table I indicate that wettability plays an important role in controlling the disturbance. To get more insights on the role of wettability, its influence on the main characteristics of the disturbance is investigated. This disturbance can be characterized by several parameters such as its mean jet radius, r^0_{jet}, its amplitude, A_d, and characteristic length, λ_d (see Fig. 7), as well as its frequency f_0. The time evolution of these parameters during the duration of the disturbance is obtained by analyzing the jet shape on the images of the movies; $r^0_{\text{jet}}(t)$, $A_d(t)$, and $\lambda_d(t)$ are extracted for each image. Since the movies are recorded at 100 fps, these parameters are obtained every 10^{-2} s throughout the jet disturbance duration.

A. Jet shape throughout the disturbance

In practice, for each recorded image the jet contour profile is extracted, allowing measurements of r^0_{jet}, A_d, and λ_d as a function of z, at time t (for details, see section 5 of the Supplemental Material [35]). These quantities, however, vary according to z due to the acceleration caused by gravity. Therefore, they are only relevant at the top of the jet, where the jet and the disturbance are not yet deformed. Consequently, values of r^0_{jet}, A_d, and λ_d, at time t, are defined as the average along the jet over the first 45 mm from the hole outlet, i.e., over the first 10 to 11 beads at the top of the jet. This z average is expressed as $\langle X(z,t)\rangle_{z\in[0,45\,\text{mm}]}$, hereafter noted $\langle X(z,t)\rangle_z$. Hence we have the following:

(i) The mean jet radius at time t is expressed as $r^0_{\text{jet}}(t) = \langle r_{\text{jet}}(z,t)\rangle_z$, where $r_{\text{jet}}(z,t)$ is the jet radius as a function of its position z and the time t.

(ii) The amplitude at time t is defined as the difference between the average of the largest, or the smallest, jet radii at time t and the mean jet radius at this time; i.e., $A_d(t) = \langle \text{Max}(r_{\text{jet}})(t)\rangle_z - r^0_{\text{jet}}(t)$ or $A_d(t) = r^0_{\text{jet}}(t) - \langle \text{Min}(r_{\text{jet}})(t)\rangle_z$. Note that $A_d(t)$ can also be written as $A_d(t) = (\langle \text{Max}(r_{\text{jet}})(t)\rangle_z - \langle \text{Min}(r_{\text{jet}})(t)\rangle_z)/2$, and this corresponds to the definition of the disturbance amplitude given above divided by two.

(iii) The characteristic length of the disturbance at time t is obtained by measuring the average distance between two consecutive pinching points at time t; i.e., $\lambda_d(t) = \langle z^{i+1}_{\text{Min}(r_{\text{jet}}(t))} - z^i_{\text{Min}(r_{\text{jet}}(t))}\rangle_z$, where $z^i_{\text{Min}(r_{\text{jet}}(t))}$ is the z location of the ith pinch at time t.

(iv) At the flow onset, $A_d(t = 0\ s)$ and $\lambda_d(t = 0\ s)$ are defined as the average value over the first 500 ms of the drainage.

The jet radius as a function of z and t can be described as follows: $r_{\text{jet}}(z,t) = r^0_{\text{jet}}(t) + \xi(z,t)$, where $\xi(z,t)$ is a function such as $|\xi(z,t)| \leqslant A_d(t)$ and $\langle \xi(z,t)\rangle_{z,t} = 0$. Time variations of ξ are fast, of the order of a few milliseconds, since their period is of the order of $\lambda_d/v_{\text{drain}}$, where $v_{\text{drain}}(t)$ is the fluid outflow velocity right at the tank outlet at time t; $\lambda_d/v_{\text{drain}} \sim 10^{-3}$ s, while time evolutions of r^0_{jet}, A_d, and λ_d, are very slow, taking place over several tens of seconds.

In all cases, it is observed the following behaviors. r^0_{jet} decreases with time and is all the larger since the wettability is high. A_d decreases on t before vanishing at the end of the disturbance; $A_d(t \approx t_{\text{stop}}) \to 0$ marks the end of the jet disturbance. As expected, the disturbance amplitude is different depending on the surface wettability; it is all the larger since the wettability is high. The disturbance characteristic length, λ_d, decreases slightly as the surface wettability decreases. For all materials, $\lambda_d(t)$ rises moderately with t before increasing sharply as the transition toward the stable regime approaches, hence as t comes close to t_{stop}. The end of the disturbed regime is therefore characterized by the disturbance amplitude that vanishes at the same time as the characteristic length diverges. These results are consistent with the disturbance description that is provided above. For four different wetting conditions with $h_0 = 10$ cm, $A_d(t = 0\ s)$, $A_d(t_{\text{stop}})$, $\lambda_d(t = 0\ s)$, and $\lambda_d(t_{\text{stop}})$, are shown in Table II. (For these wetting conditions, typical time evolutions of A_d and λ_d are displayed in section 6 of the Supplemental Material [35].)

TABLE II. For four wetting conditions and with the same initial height of fluid in the tank: $h_0 = 10$ cm, measured values of the at the flow onset, $A_d(t = 0\ s)$ ($A_d(t = 0\ s)$ is the average value of $A_d(t)$ over the first 500 ms of the drainage) in Column 1; disturbance amplitude when the disturbance vanishes at $t = t_{\text{stop}}$, $A_d(t_{\text{stop}})$ in Column 2; disturbance characteristic length at the flow onset, $\lambda_d(t = 0\ s)$ ($\lambda_d(t = 0\ s)$ is the average value of $\lambda_d(t)$ over the first 500 ms of the drainage) in Column 3; disturbance characteristic length at $t = t_{\text{stop}}$, $\lambda_d(t_{\text{stop}})$ in Column 4.

Material	$A_d(t = 0\ s)$ (mm)	$A_d(t_{\text{stop}})$ (mm)	$\lambda_d(t = 0\ s)$ (mm)	$\lambda_d(t_{\text{stop}})$ (mm)
Hydrophilic glass ($\theta_s \sim 13°$)	0.55 ± 0.05	0	3.8 ± 0.2	∞
Plexiglas ($\theta_s \sim 64°$)	0.40 ± 0.05	0	3.6 ± 0.2	∞
PVC-1 ($\theta_s \sim 68°$)	0.34 ± 0.05	0	3.5 ± 0.2	∞
Hydrophobic glass ($\theta_s \sim 88°$)	0.08 ± 0.01	0	3.3 ± 0.2	∞

In Fig. 8, A_d and λ_d obtained for a hydrophilic glass plate are plotted as a function of t and h for different initial heights of water in the tank; $h_0 = 11$, 9, 7, 5 cm, respectively. Of course, the disturbance duration, t_{stop}, is all the shorter since h_0 is close to h^*. In the same way, the t_{stop}-t_{drain} ratio decreases with h_0. $A_d(t = 0\ s)$ decreases with h_0, whereas $\lambda_d(t = 0\ s)$ increases as h_0

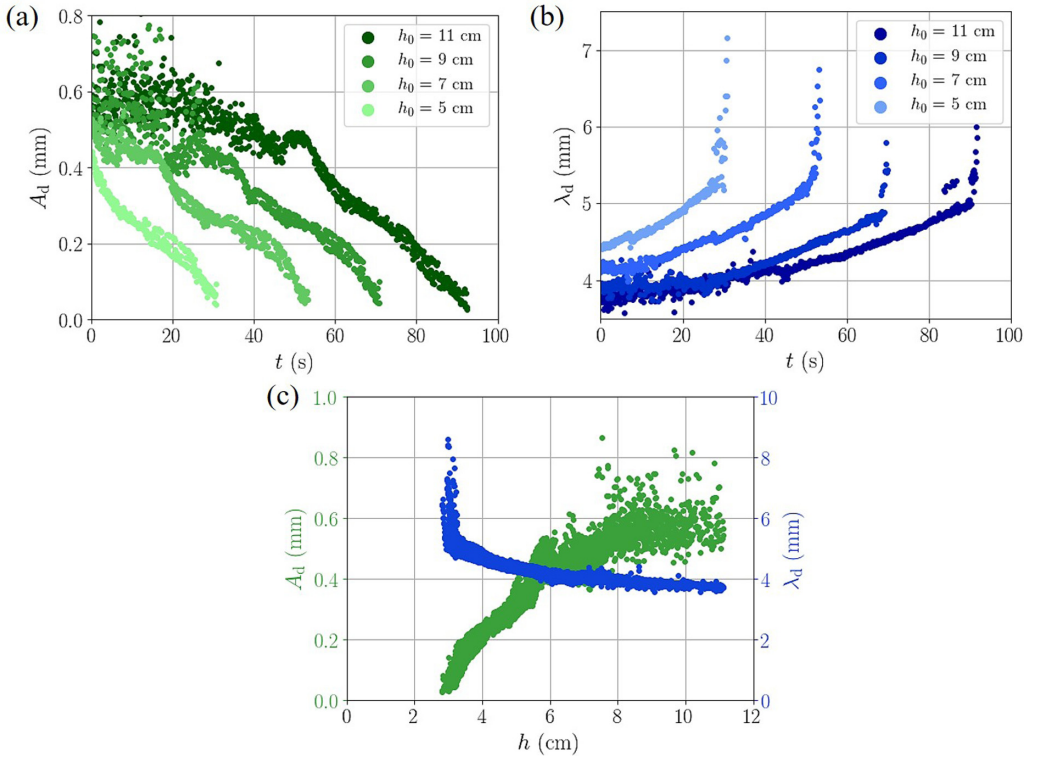

FIG. 8. Measured amplitude A_d and characteristic length λ_d of the jet disturbance as a function of time t [(a) and (b)] and the remaining height of fluid in the tank h (c) for $h_0 = 11, 9, 7, 5$ cm, respectively. Results obtained in the case of a hydrophilic glass surface ($r_0 = 1.75$ mm, water). (Results obtained for flows of water through a PVC plate are shown in section 6 of the Supplemental Material [35].)

TABLE III. For all wetting conditions. Column 1: h^*, estimated values of the threshold height; $h^* = \langle h_{\text{stop}} \rangle$, where $\langle h_{\text{stop}} \rangle$ is average value of the fluid height remaining in the tank when the disturbance vanishes measured over all experiments carried out with 11 cm $\geqslant h_0 \geqslant$ 2 cm. Column 2: P_H^*, estimated values of the threshold hydrostatic pressure. Column 3: v^*, estimated values of the threshold flow velocity, Q_{stop} is the measured values of the flow rate at h_{stop}, or $t = t_{\text{stop}}$; $Q(h_{\text{stop}})$ or $Q(t_{\text{stop}})$.

Material	$h^* = \langle h_{\text{stop}} \rangle$ (cm)	$P_H^* = \rho g \langle h_{\text{stop}} \rangle$ (Pa)	$v^* = \langle Q_{\text{stop}} \rangle / (\pi r_0^2)$ (m s^{-1})
Hydrophilic glass ($\theta_s \sim 13^\circ$)	3.0 ± 0.1	295 ± 15	0.62 ± 0.01
Plexiglas ($\theta_s \sim 64^\circ$)	4.5 ± 0.1	441 ± 15	0.67 ± 0.01
PVC-1 ($\theta_s \sim 68^\circ$)	5.5 ± 0.1	538 ± 15	0.73 ± 0.01
PVC-2 ($\theta_s \sim 70^\circ$)	5.9 ± 0.1	568 ± 15	0.75 ± 0.01
Hydrophobic glass ($\theta_s \sim 88^\circ$)	7.8 ± 0.1	765 ± 15	0.93 ± 0.01

decreases. These behaviors are consistent with those described above. Figure 8(c) displays A_d and λ_d as a function of h for the different h_0. It is seen that all obtained data superimpose on a master curve; for both $A_d(h)$ (in green) and $\lambda_d(h)$ (in blue). The same behavior is observed for all wetting conditions (e.g., see PVC results in section 6 of the Supplemental Material [35]). Therefore, for a given surface wettability, the amplitude and the characteristic length of the jet disturbance only depend on the remaining fluid height in the tank h and not on the initial conditions. Moreover, the disturbance always disappears for the same remaining fluid height in the tank; whatever $h_0 > h^*$, the perturbation vanishes as h reaches h_{stop}. These latter observations suggest a lack of memory effect. This is understandable since the macroscopic variations of the disturbance are very slow with respect to the time required to establish it (i.e., quasi-steady-state regime). This is confirmed by the fact that $Q(h)$ is always independent of h_0, this both in the disturbed regime and the stable regime (see section 7 of the Supplemental Material [35]). Thus the time dependence of this disturbance is indeed an artifact of the experimental device since the pressure head decreases as water flows out. A tank of different width would give a different time dependence; keeping h constant in the tank would provide a disturbance with constant characteristics. However, this allows us to make Q and P_H evolve with time to investigate the effect of their value on the disturbance.

Measurements of A_d and λ_d allow estimation of h_{stop} for each surface wettability. According to these measurements, h_{stop} seems to be equal to h^*; at least, they are very close and cannot be distinguished, when $h_0 > h^*$, $h_{\text{stop}} \approx h^*$. Consequently, for a given wettability v_{stop} and $P_{H\text{stop}}$ are constant with h_0. The threshold height, threshold velocity, and threshold hydrostatic pressure are defined as $h^* = \langle h_{\text{stop}} \rangle$, $v^* = \langle Q_{\text{stop}} \rangle / (\pi r_0^2)$, and $P_H^* = \rho g \langle h_{\text{stop}} \rangle$. For all investigated wettability, values of h^*, h_{stop}, v^*, and P_H^* are displayed in Table III. The effect of surface wettability on the disturbed-stable regime transition is obvious.

B. Disturbance frequency

The disturbance frequency f_0 is defined as the frequency of the bead appearance at the top of the jet, i.e., $f_0 = 1/\tau_0$.

In the context of a continuous string of beads produced at the hole outlet, the volume flow rate has to be written as $Q = f_0 V_b$, where V_b is the bead volume. Values of V_b can be estimated using the images of the jet by taking the shape and area of the beads and assuming a circular symmetry. According to this analysis, V_b seems to be constant with h_0 and time, as long as the remaining fluid height in tank h is not too close to h_{stop}. Therefore, as V_b is constant for most of the disturbance, it should imply that f_0 is only monitored by the outflow velocity of the fluid right at the tank outlet;

thus

$$f_0(t) = \pi r_0^2 \frac{v_{\text{drain}}(t)}{V_b}. \tag{1}$$

Following the idea of annular vortices created by the detachment of the boundary layer at the entrance of the hole, one can imagine that f_0 can be written as $f_0 = \text{St} v_{\text{drain}}/D$, where St is the Strouhal number and D a characteristic length. The Strouhal number is a dimensionless number that is often used to characterize oscillating flow mechanisms; it represents the ratio of inertial forces due to the unsteadiness of the flow to the inertial forces due to the convective acceleration. For the characteristic length D, the simplest idea is to take the hole diameter, $D = 2r_0$. Hence, it can be expected: $f_0 = \text{St} v_{\text{drain}}/2r_0$. In this framework also f_0 is expected to be proportional to v_{drain}. Combining both approaches, $\text{St} = 2\pi r_0^3/V_b$.

Thereby, for most of the disturbance duration, f_0 is expected to vary identically to v_{drain} that can be estimated according to experimental parameters simply. Indeed, $v_{\text{drain}}(t)$, is often written as [3–8] $v_{\text{drain}}(t) = \sqrt{2Cgh(t)}$, where C is a constant smaller than 1 that takes into account dissipation effects and $h(t)$ is the height of fluid in the tank at time t. However, here the outflow velocity is best described by $v_{\text{drain}}(t) = \sqrt{2Cg(h(t) - \delta h_0)}$ (see section 7 of the Supplemental Material [35]). Such an expression is provided in Ref. [10]; it simply arises from the Bernouilli's equation with two sources of dissipation: the minor head losses, occurring when a fluid flows out from a tank with a large cross-sectional area (C), and an additional dissipation arising from the jet contraction induced by the detachment of the boundary layer (δh_0). Using this latter expression of v_{drain}, it is possible to express f_0 as a function of h as

$$f_0(h) = \frac{\pi r_0^2}{V_b}\sqrt{2Cg}\sqrt{h(t) - \delta h_0} = \frac{\text{St}}{2r_0}\sqrt{2Cg}\sqrt{h(t) - \delta h_0}. \tag{2}$$

Either still

$$f_0^2(h) = 2Cg\frac{\pi^2 r_0^4}{V_b^2}(h - \delta h_0) = 2Cg\frac{\pi^2 r_0^4}{V_b^2}h - 2Cg\frac{\pi^2 r_0^4}{V_b^2}\delta h_0, \tag{3}$$

which can also be written as

$$f_0^2(h) = \frac{\text{St}^2}{2r_0^2}Cgh - \frac{\text{St}^2}{2r_0^2}Cg\delta h_0. \tag{4}$$

Furthermore, time evolution of f_0 can be calculated by replacing $h(t)$ by its expression as a function of t. The quantity $h(t)$ can be calculated by writing the flow rate conservation between the fluid free surface and the outlet hole

$$\frac{dh}{dt} = -\frac{\pi r_0^2}{a^2}\sqrt{2Cg(h(t) - \delta h_0)}, \tag{5}$$

where a^2 is the tank area. Integrating this latter equation leads to

$$h(t) = h_0 - \frac{\pi r_0^2\sqrt{2Cg(h_0 - \delta h_0)}}{a^2}t + \frac{\pi^2 r_0^4}{2a^4}Cgt^2. \tag{6}$$

Therefore, the volume flow rate at time t, $Q(t)$, is

$$Q(t) = -a^2\frac{dh(t)}{dt} \;\Leftrightarrow\; Q(t) = \pi r_0^2\sqrt{2Cg(h_0 - \delta h_0)} - \frac{\pi^2 r_0^4}{a^2}Cgt. \tag{7}$$

Thus

$$f_0(t) = \frac{\pi r_0^2}{V_b}\sqrt{2Cg(h_0 - \delta h_0)} - \frac{\pi^2 r_0^4}{a^2 V_b}Cgt = \frac{\text{St}}{2r_0}\sqrt{2Cg(h_0 - \delta h_0)} - \frac{\pi r_0 \text{St}}{2a^2}Cgt. \tag{8}$$

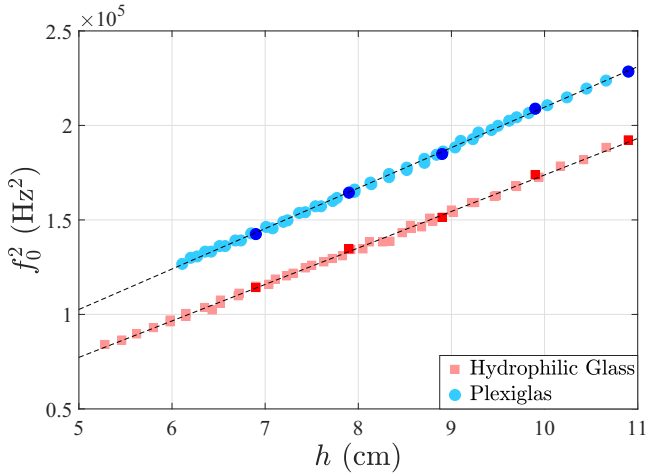

FIG. 9. f_0^2 as a function of h: (red) hydrophilic glass ($\theta_s \approx 13°$) and (blue) Plexiglas ($\theta_s \approx 64°$). Error bars on measured values of f_0 are smaller than used symbols. Dark symbols represent the measured values of f_0 at the onset of the flows for $h_0 = 11$, 10, 9, 8, and 7 cm, respectively. There f_0 is obtained over the first 2 s of the draining process. Light symbols correspond to frequencies measured at different times throughout the first 24 s of the draining for the different h_0. Here h is the average over 2 s of $h(t)$ deduced from the measurement of the drained volume $V(t)$ [note that $h(t-1\,s) - h(t+1\,s) \leqslant 2$ mm], while f_0 is obtained over the same 2 s. $f_0^2(\theta_s) = \alpha(\theta_s)[h - \delta h_f(\theta_s)]$ with $\alpha(13°) \approx (17500 \pm 600)$ Hz^2 cm^{-1}, $\delta h_f(13°) \approx (0.315 \pm 0.015)$ cm, and $\alpha(64°) \approx (21300 \pm 750)$ Hz^2 cm^{-1}, $\delta h_f(64°) \approx (0.145 \pm 0.010)$ cm.

Analysis of the experimental results provides values of $C < 1$ and δh_0 of the order of a few millimeters. As already mentioned, parameters C and δh_0 allow us to consider all dissipation and wetting effects; they depend on the outer surface wettability, which agrees with Ref. [20] but are constants with h_0 for a given material.

The frequency spectrum of the jet disturbance at its top and at time t is determined by doing a short-time Fourier transform of the signal $r_{\text{jet}}(z, \tau)$, in $z = 4$ mm, over a 2-s time window around time t. Values of $r_{\text{jet}}(z = 4\text{ mm}, \tau)$ are obtained by using movies of the jet disturbances recorded at 6000 fps thanks to the high-speed camera. This allows us to measure time-frequency spectra [33] of the jet disturbance at its top over the first 24 s of the draining process. These measurements are carried out for different values of the initial fluid height in the tank; $h_0 = 11$, 10, 9, 8, and 7 cm, respectively, both for the hydrophilic glass surface and the Plexiglas surface (see details in section 8 of the Supplemental Material [35]). In all cases, only a single frequency corresponding to the characteristic time of the bead appearance τ_0 is observed, $f_0 = 1/\tau_0$. This frequency decreases linearly with time, which agrees with what is expected from Eq. (8). Figure 9 displays the square of the measured frequencies, f_0^2, as a function of h for the different h_0. For a given material, whatever the value of h_0, all the measured frequencies place themselves on a master curve. f_0 only depends on h and not on h_0; it is a further indication that there is no memory effect. f_0^2 is a linear function of h, in agreement with Eq. (3). This clearly demonstrates that f_0 is proportional to v_{drain}. As expected (see last paragraph of Sec. III), f_0 is smaller for the hydrophilic glass surface than for the Plexiglas surface. This may appear surprising, since the outlet velocity of the fluid is slightly higher for the hydrophilic glass surface than for the Plexiglas surface [20], very likely this is because the bead volume V_b is greater for the hydrophilic glass surface. All these observations are in concordance with what is expected.

f_0^2 is written as $f_0^2(\theta_s) = \alpha(\theta_s)[h - \delta h_f(\theta_s)]$, where $\alpha(\theta_s)$ and $\alpha(\theta_s)\delta h_f(\theta_s)$ are respectively the slope and the intercept of this linear function for the material of wettability θ_s. Identifying

parameters $\alpha(\theta_s)$ and $\delta h_f(\theta_s)$ with coefficients of Eq. (3) leads to $\sqrt{\alpha(\theta_s)} = \pi r_0^2\sqrt{2Cg}/V_b(\theta_s)$, and $\delta h_f(\theta_s) = \delta h_0$.

(i) For hydrophilic glass, $\delta h_f \approx 3.15 \pm 0.15$ mm, while for Plexiglas $\delta h_f \approx 1.45 \pm 0.10$ mm. Such estimated values of δh_f are in accordance with those of δh_0 deduced from the fitting of $Q(t)$ or $V(t)$; $\delta h_0 \approx 3.25 \pm 0.10$ mm and $\approx 1.5 \pm 0.1$ for hydrophilic glass and Plexiglas, respectively.

(ii) Values of $V_b(\theta_s)$ may be estimated by combining obtained values of $\alpha(\theta_s)$ and those of $C(\theta_s)$ provided by fitting $Q(t)$ or $V(t)$ [$C(13^\circ) = 0.79$ and $C(64^\circ) = 0.59$]; $V_b \approx 2.86 \times 10^{-8}$ m^3 ($\sim$28.6 μl) for hydrophilic glass, and $V_b \approx 2.25 \times 10^{-8}$ m^3 ($\sim$22.5 μl) for Plexiglas. In agreement with observations (e.g., in Fig. 2 or Fig. 4), V_b is found to be greater for hydrophilic glass than for Plexiglas. V_b can also be estimated simply as the ratio Q-f_0 or calculated using the images of the jet by taking the shape and area of the beads and assuming a circular symmetry. Regardless of the method used to estimate V_b, for both materials, it is observed that the values of V_b are constant as a function of h over the entire range of fluid height over which f_0 is measured (see section 9 of the Supplemental Material [35]). The average values of V_b over all values of h are $V_b \approx 2.86 \times 10^{-8}$ m^3 ($\sim$28.6 μl), or $\approx 3 \times 10^{-8}$ m^{-3} (30 μl), for hydrophilic glass surface and $V_b \approx 2.25 \times 10^{-8}$ m^3 ($\sim$22.5 μl), or $\approx 2.35 \times 10^{-8}$ m^{-3} (23.5 μl), for the Plexiglas surface. Thus, all sets of estimated values of V_b are in the same order of magnitude.

(iii) Using the bead area to determine V_b makes it possible to estimate its evolution as a function of h. At first, V_b is constant over a broad range of h; however, as h is approaching h_{stop}, V_b slightly decreases and then sharply increases at the very end of the disturbance. The frequency f_0 was not measured for h close to h_{stop}; however, one can expect that f_0^2 does not remain a linear function of h for the whole disturbance duration. Likely, this does not hold any more for h smaller than, typically, $\sim h_{\text{stop}} + 1.5$ cm. Nevertheless, we believe that Eq. (3) still works but with V_b varying as a function of h.

(iv) $\text{St} = 2\pi r_0^3/V_b$, hence, during most of the disturbance duration, as long as V_b is constant with h, St is constant. In this regime, it is found St $\approx$1.13 for hydrophilic glass and St $\approx$1.44 for Plexiglas. However, when V_b increases sharply as the end of the perturbation approaches, St is expected to decrease and tend toward 0. This leads to f_0 going to 0 as the disturbance vanishes, which is what is observed.

C. Critical dimensionless numbers

The Strouhal number describes well the transition between the disturbed jet and the stable jet. The Strouhal number, however, depends on V_b, which is a parameter we do not control. Can it be found out a critical dimensionless number, depending in the control parameters, that describes the transition between the two states? Of course, because of the origin of the disturbance, one could think of a critical Reynolds number, Re*. However, it is observed that Re* depends on the surface wettability. Values of the dimensionless numbers usually used to characterize jets are estimated at the transition between the disturbed and the stable jet. Critical values of the Reynolds, Weber, Froude, and capillary numbers are calculated as follows:

$$\text{Re}^* = \frac{2r_0\rho v^*}{\eta}; \quad \text{We}^* = \frac{2r_0\rho v^{*2}}{\gamma}; \quad \text{Fr}^* = \frac{v^{*2}}{2gh^*}; \quad \text{Ca}^* = \frac{\eta v^*}{\gamma} = \frac{\text{We}^*}{\text{Re}^*},$$

where v^* is the fluid outlet velocity at which the jet disturbance disappears.

The behavior of Re*, We*, Fr*, and Ca* is considered for the different wetting conditions. For all wettability, the estimated values are displayed in Table IV. None of these dimensionless numbers is constant on wettability at the disappearance of the disturbance. Consequently, none of these dimensionless numbers can characterize the transition between the disturbed jet and the stable jet. Nevertheless, this is not surprising that they are all different for all wetting conditions. Re*, We*, and Ca* are proportional to v^* or v^{*2} and depend on ρ, η, γ, and r_0. v^* depends on the wettability of the outer surface of the bottom plate, while ρ, η, γ, and r_0, are constant in all cases since for all experiments are carried out with water and a hole radius which is identical. Therefore, as the

TABLE IV. For all wetting conditions, h_0 varying between 2 and 11 cm. Column 1: Re*, estimated values of the Reynolds number at the transition between the disturbed jet and the stable jet. Column 2: We*, estimated values of the Weber number at the transition between the disturbed jet and the stable jet. Column 3: Fr*, estimated values of the Froude number at the transition between the disturbed jet and the stable jet. Column 4: Ca*, estimated values of the Capillary number at the transition between the disturbed jet and the stable jet.

Material	Re*	We*	Fr*	Ca*
Hydrophilic glass ($\theta_s \sim 13°$)	∼2180	∼19	∼ 0.67	$\sim 8.7 \times 10^{-3}$
Plexiglas ($\theta_s \sim 64°$)	∼2350	∼22	∼0.51	$\sim 9.3 \times 10^{-3}$
PVC-1 ($\theta_s \sim 68°$)	∼2560	∼26	∼0.50	$\sim 10.2 \times 10^{-3}$
PVC-2 ($\theta_s \sim 70°$)	∼2600	∼27	∼0.49	$\sim 10.4 \times 10^{-3}$
Hydrophobic glass ($\theta_s \sim 88°$)	∼3250	∼42	∼0.56	$\sim 13.0 \times 10^{-3}$

evolution of v^*, these numbers increase as the outer surface wettability decreases. Fr* is not constant as well and exhibits a nonmonotone behavior according to the surface wettability; this indicates that C and δh_0 depend on the wettability, in agreement with the results previously displayed.

Other dimensionless numbers can be constructed based on the previous numbers, e.g., the Ohnesorge number:

$$\mathrm{Oh}^* = \frac{\sqrt{\mathrm{We}^*}}{\mathrm{Re}^*} = \frac{\eta}{\sqrt{2 r_0 \rho \gamma}}.$$

Either these dimensionless numbers only depend on ρ, η, γ, and r_0 and are thus always constant (such as Oh), which means nothing, or they also depend on v^* and then they are different for the different wettability. Surface wettability plays an important role in this disturbance and none of the dimensionless numbers we could build considers this parameter. Therefore, they cannot characterize the transition toward the stable regime. To be able to characterize this transition, a dimensionless number must be determined that considers the surface wettability. Unfortunately, we did not manage to build such a number.

In conclusion, all the results shown in Sec. V confirm the important role of surface wettability in this phenomenon. Surface wettability, indeed, controls the disturbance amplitude, but it also monitors the existence of the disturbance as well as the transition to the stable jet state, the fluid outlet velocity during the disturbance, the process of bead appearance, and thereby the disturbance frequency.

VI. CONCLUSION

In this article, we describe and characterize what we believe to be a new type of jet disturbance that has never been reported before. At first sight, this perturbation is characterized by a regular pinching of the jet along the z axis, which causes the jet to exhibit a string of beads. From our experimental results, we conclude that this disturbance is in no way a known jet instability.

This disturbance occurs during tank draining for flows through a sharp edge circular hole, whose size is comparable to the capillary length, when the initial fluid height in the tank exceeds a threshold value. Further investigations that were carried out and not shown in this article [34] indicate that with the used experimental setup, the different wettability and $11 \geqslant h_0 \geqslant 2$ cm, the disturbance may exist for hole radii between 1 and 4 mm. For radius below 1 mm, the flow is by drip, for a radius greater than 4 mm, the jet becomes highly turbulent, the effects of wetting become marginal, and the disturbance is not visible. As the initial fluid height in the tank has to exceed a threshold value, this perturbation only exists if the initial fluid outlet velocity is higher than a threshold velocity or if the initial hydrostatic pressure is above a threshold hydrostatic pressure. This threshold velocity, or this threshold hydrostatic pressure, depends on the surface wettability; it is all the smaller since

the surface is hydrophilic. Moreover, according to the estimated Reynolds number values in the disturbed regime, the disturbed flow is expected to be turbulent, which is observed. If the initial fluid outlet velocity-initial hydrostatic pressure is higher than its threshold value, then this jet disturbance occurs at the tank outlet level as soon as the hole is opened. This disturbance is always fully set in a few tens of milliseconds after the flow onset, typically in about 25–30 mms. It disappears as soon as the fluid outlet velocity-hydrostatic pressure goes below its threshold value. This disturbance can last for several tens of seconds and therefore up to four orders of magnitude in time. If the initial fluid outlet velocity-initial hydrostatic pressure is smaller than its threshold value, then there is no disturbance. It is observed that for a given h_0 larger than h^*, this disturbance develops even more and lasts all the longer since the surface is hydrophilic. Thereby this jet disturbance is monitored by a few parameters only, among which fluid outlet velocity-hydrostatic pressure, as well as wettability of the outer surface around the outlet hole, seem to be the most important.

Beads appear at the hole outlet and then are advected by the flow that falls in free fall due to gravity. The process of bead appearance is very fast, a few milliseconds. The results of this study lead us to believe that each bead is a vortex ring produced at the inlet of the outlet hole. In this framework, this jet disturbance is due to the interplay between wetting and turbulence. In other words, we feel that this disturbance originates from the combination of toroidal turbulence at the inlet of the outlet hole and wettability of the outer surface around the outlet orifice. The turbulence arises from the boundary layer detachment at the entrance of the outlet orifice, the toroidal vortices thus created wet the outer solid surface when popping out of orifice outlet and then the disturbance can develop. When turbulence stands at the inlet of the outlet hole, the outer surface wettability controls the existence and disappearance of the disturbance. In the disturbed regime, r_{jet}^0, A_d, and λ_d, as well as f_0, depend on surface wettability and vary with the height of fluid as well; hence, with the fluid outlet velocity or the hydrostatic pressure.

This disturbance is, therefore, a signature of the effects of wetting on the draining of a reservoir through a circular hole the size of which is of the order of magnitude of the fluid capillary length, κ^{-1}. More experiments are of course necessary for a full understanding of this disturbance, but most importantly, a theoretical description of this phenomena would be an essential complement to the experimental investigations.

ACKNOWLEDGMENTS

The authors thank Dr. Jean-Christophe Géminard and Dr. Christophe Raufaste for their fruitful discussions, Dr. Nicolas Plihon for lending us the high-speed camera, as well as Franck Vittoz for designing and building the tank.

[1] E. Torricelli, *Opera Geometrica; De motu gravium* (A. Maffe & L. J de Landis, Florentiae, 1644), pp. 191–204.

[2] D. Bernoulli, *Hydrodynamica, sive De Viribus et Motibus Fluidorum Commentarii: Opus Academicum* (Dulsecker, Strasbourg, 1738).

[3] R. Ouziaux and J. Perrier, *Mécanique des fluides appliquée–Tome 1–Fluides incompressibles* (Dunod, Paris, 1966).

[4] J. Boussinesq, Essai sur la théorie de l'écoulement d'un liquide par un orifice en mince paroi, C. R. Acad. Sci. Paris **70**, 33 (1870).

[5] H. von Helmholtz, Über discontinuirliche flüssigkeigt–bewegungen, Monatsberich. Königlich. Preuss. Akad. Wissenschaft. Berl. **23**, 215 (1868).

[6] P. Forchheimer, *Hydraulik* (B. G. Teubner, Leipzig, 1914), pp. 341–343.

[7] G. F. Davidson, Experiments on the flow of viscous fluids through orifices, Proc. R. Soc. Lond. **89**, 91 (1913).

[8] C. Clanet, Clepsydrae, from galilei to torricelli, Phys. Fluids **12**, 2743 (2000).

[9] M. E. Saleta, D. Tobia, and S. Gil, Experimental study of bernoulli's equation with losses, Am. J. Phys. **73**, 598 (2005).
[10] T. Massalha and R. M. Digilov, Experimental evidence of capillary interruption of a liquid jet, Open J. Appl. Sci. **4**, 392 (2014).
[11] T. Young, An essay on the cohesion of fluids, Philos. Trans. R. Soc. Lond. **95**, 65 (1805).
[12] P. G. de Gennes, Wetting: Statics and dynamics, Rev. Mod. Phys. **57**, 827 (1985).
[13] R. J. Good, Contact-angle, wetting, and adhesion—A critical review, J. Adhes. Sci. Technol. **6**, 1269 (1992).
[14] D. Quéré, Wetting and roughness, Annu. Rev. Mater. Res. **38**, 71 (2008).
[15] T. Blake and K. Ruschak, A maximum speed of wetting, Nature (Lond.) **282**, 489 (1979).
[16] S. F. Kistler and L. E. Scriven, Coating flows, in *Computational Analysis of Polymer Processing*, edited by J. R. A. Pearson and S. M. Richardson (Applied Science Publishers, Amsterdam, 1983), pp. 243–299.
[17] S. F. Kistler and L. E. Scriven, The teapot effect: Sheet-forming flows with deflection, wetting and hysteresis, J. Fluid Mech. **263**, 19 (1994).
[18] C. Duez, C. Ybert, C. Clanet, and L. Bocquet, Making a splash with water repellency, Nat. Phys. **3**, 180 (2007).
[19] C. Duez, C. Ybert, C. Clanet, and L. Bocquet, Wetting Controls Separation of Inertial Flows From Solid Surfaces, Phys. Rev. Lett. **104**, 084503 (2010).
[20] J. Ferrand, L. Favreau, S. Joubaud, and E. Freyssingeas, Wetting Effect on Torricelli's Law, Phys. Rev. Lett. **117**, 248002 (2016).
[21] C. Clanet and J. C. Lasheras, Transition from dripping to jetting, J. Fluid Mech. **383**, 307 (1999).
[22] According to the Young-Dupré equation; $\gamma \cos\theta_s = \gamma_{SG} - \gamma_{SL}$, where γ_{SG} and γ_{SL} are the solid-gaz and solid-liquid interfacial energies, respectively.
[23] J. Eggers and E. Villermaux, Physics of liquid jets, Rep. Prog. Phys. **71** (2008).
[24] E. Guyon, J.-P. Hulin, L. Petit, and C. D. Mitescu, *Physical Hydrodynamics*, 2nd ed. (Oxford University Press, Oxford, 2015), p. 302.
[25] C. Kouris and J. Tsamopoulos, Dynamics of axisymmetric core-annular flow in a straight tube. i. The more viscous fluid in the core, bamboo waves, Phys. Fluids **13**, 841 (2001).
[26] G. Ooms, C. Vuik, and P. Poesio, Core-annular flow through a horizontal pipe: Hydrodynamic counter-balancing of buoyancy force on core, Phys. Fluids **19**, 092103 (2007).
[27] S. Ghosh, T. Mandal, G. Das, and P. Das, Review of oil water core annular flow, Renew. Sust. Energy Rev. **13**, 1957 (2009).
[28] M. P. Wilson Jr. and R. G. Teyssandier, The paradox of the vena contracta, J. Fluids Eng. **97**, 366 (1975).
[29] F. Durst, W. F. Schierholz, and A. M. Wunderlich, Experimental and numerical investigations of plane duct flows with sudden contraction, J. Fluids Eng. **109**, 376 (1987).
[30] A. Habibzadeh, A. R. Vatankhah, and N. Rajaratnam, Role of energy loss on discharge characteristics of sluice gates, J. Hydraul. Eng. **137**, 1079 (2011).
[31] J. E. Borges, M. Lourenço, E. L. Padilla, and C. Micallef, Immersed boundary method application as a way to deal with the three-dimensional sudden contraction, Computation **6**, 50 (2018).
[32] T. Schnipper, A. Andersen, and T. Bohr, Vortex wakes of a flapping foil., J. Fluid Mech. **633**, 411 (2009).
[33] P. Flandrin, *Time-Frequency/Time-Scale Analysis* (Academic Press, San Diego, CA, 1999).
[34] L. Favreau, Écoulements forcés par gravité de fluides simples et de fluides complexes, edited by E. N. S. de Lyon, Ph.D. thesis, université de Lyon, Lyon, 2020.
[35] See Supplemental Material at http://link.aps.org/supplemental/10.1103/PhysRevFluids.7.014002 for experimental details, movies, pictures, and additional measurements. Notations are the same as in the present paper, which includes Ref. [20].